Meas. Sci. Technol. 1 (1990) 59–64. Printed in the UK

Holographic focusing elements for far-IR radiation

E Hasman,† N Davidson,† A A Friesem,† M Nagler‡ and R Cohen‡

† The Department of Electronics, Weizmann Institute of Science, Rehovot 76100, Israel
‡ Scitex Corp., Herzlia B 46103, Israel

Received 6 April 1989, accepted for publication 11 July 1989

Abstract. This paper presents a method for designing and recording computer-generated holographic optical elements (HOEs) for far-infrared radiation. The design method is based on minimising the mean-squared difference of the propagation vectors between the actual output wavefronts and the desired output wavefronts. This minimisation yields an analytic solution for the optimal grating vector. The design method is illustrated by recording a reflective off-axis focusing element with a laser scanner and lithographic techniques. The element is then tested, and the results indicate that diffraction-limited performance for a relatively large range of incidence angles can be obtained.

1. Introduction

Since there are no practical recording materials for far-infrared (IR) radiation, holographic optical elements (HOEs) must be formed by using indirect recording [1–4]. Specifically, the elements can be recorded holographically with visible radiation [2,3] or by means of computer-generated holograms [4], and the readout is performed with IR. Holographic recording produces severe geometric aberrations associated with the large wavelength shift between recording and readout of the hologram. It is possible to design aberration-free holographic elements for only a single image point [2,3]. However, other points will be marred by severe aberrations. Computer generated holograms (CGHs), on the other hand, make it possible to alleviate the aberrations by recording more complicated gratings.

In order to record a HOE as a CGH so as to have minimum geometric aberrations in readout, it is necessary to exploit optimisation procedures for designing a holographic element having a complicated grating. We have developed an optimisation procedure [5,6] in which the design is based on analytic ray-tracing which minimises the mean-squared difference of the propagation vector components between the actual output wavefronts and the desired output wavefronts. This procedure leads to the HOE having an optimised grating function. In practice, a computer-generated mask, representing the grating function, is first plotted with a laser scanner, then reduced in size by optical demagnification and finally recorded as a relief pattern with photolithographic techniques.

We shall illustrate the design and recording techniques with reflective off-axis focusing elements for a readout wavelength of 10.6 μm from the CO_2 laser. The elements can have diffraction-limited spot sizes for incident plane waves with relatively large incidence angles. Section 2 describes the theoretical analysis of the design procedure for general holographic optical elements, and § 3 illustrates the design procedure for a specific focusing element that operates with IR. The realisation of this focusing element and the experimental performance results are given in § 4. Finally, concluding remarks are given in § 5.

2. The optimisation procedure

The holographic optical element can be described as a diffractive grating that transforms the phase of an incoming wavefront to another output phase. The phase of the output wavefront, $\psi_o(x, y)$, for the first diffracted order is given by

$$\psi_o(x, y) = \psi_i(x, y) - \psi_h(x, y) \tag{1}$$

where $\psi_i(x, y)$ is the phase of the input wavefront and $\psi_h(x, y)$ is the grating function of the HOE.

To proceed, we will now exploit the normalised propagation vectors and grating vector of the holographic element, rather than the phases. The normalised propagation vectors, which can be regarded as the direction cosines of the input ($\hat{K}_i$) and output ($\hat{K}_o$) rays, can be written as

$$\hat{K}_o = \frac{\lambda}{2\pi}\nabla\psi_o \quad \text{and} \quad \hat{K}_i = \frac{\lambda}{2\pi}\nabla\psi_i \tag{2}$$

and the grating vector $\bar{K}_h$ as

$$\bar{K}_h = \frac{\lambda}{2\pi}\nabla\psi_h = \frac{\lambda}{\Lambda_x}\hat{x} + \frac{\lambda}{\Lambda_y}\hat{y} \tag{3}$$

0957-0233/90/010059 + 06 $03 50

where $\bar{\nabla}$ is the gradient operator, Λ_x and Λ_y are grating spacing in x and y directions [7], and λ is the readout wavelength. The diffraction relations can now be written as

$$\hat{K}_{x_o} = \hat{K}_{x_i} - K_{x_h} \tag{4}$$

$$\hat{K}_{y_o} = \hat{K}_{y_i} - K_{y_h} \tag{5}$$

$$\hat{K}_{z_o} = \pm\sqrt{1 - \hat{K}_{x_o}^2 - \hat{K}_{y_o}^2}. \tag{6}$$

Note that $\hat{K}_{x_o}^2 + \hat{K}_{y_o}^2$ should be less than one so as not to obtain evanescent wavefronts.

The goal when designing HOEs is to transfer input rays into corresponding output rays that will be optimised for a given range of input parameters. The input parameter could, for example, be the direction cosine of the incoming waves, or the location of the input point sources. For a single specific input parameter it is relatively easy to form a HOE that will yield the exact desired output rays. However, for a range of input parameters, it is necessary to optimise the grating vector so as to minimise the difference between the actual and the desired output rays. The optimisation is achieved by minimising the mean-squared difference between these two sets of rays.

To simplify the presentation of our optimisation method, we will describe the method in one-dimensional notation. The mean-squared difference of the propagation vectors is defined as

$$E^2 = \int_{-D}^{D}\int_{a_1(x)}^{a_2(x)} (\hat{K}_{x_d}(x, a) - \hat{K}_{x_o}(x, a))^2 \, da \, dx \tag{7}$$

where the direction cosines of the output and desired rays, $\hat{K}_{x_o}(x, a)$ and $\hat{K}_{x_d}(x, a)$, depend on some input parameter a, and x is the space coordinate on the HOE. The limits of integration, $a_1(x)$ and $a_2(x)$, represent the upper and lower values of the parameter of the input waves that intercept the HOE at a point x. The holographic element aperture is 2D. Inserting equation (4) into (7), yields

$$E^2 = \int_{-D}^{D}\int_{a_1(x)}^{a_2(x)} (\hat{K}_{x_d}(x, a) - \hat{K}_{x_i}(x, a) + K_{x_h}(x))^2 \, da \, dx \tag{8}$$

The optimal grating vector component $K_{x_h}(x)$, can be determined by minimising E^2. However, because the integrand is always positive, it is sufficient to minimise a simpler integral that we denote as $e^2(x_o)$:

$$e^2(x_o) = \int_{a_1(x_o)}^{a_2(x_o)} (\hat{K}_{x_d}(x_o, a) - \hat{K}_{x_i}(x_o, a) + K_{x_h}(x_o))^2 \, da \tag{9}$$

where x_o represents an arbitrary coordinate x. Differentiating $e^2(x_o)$ with respect to $K_{x_h}(x_o)$ and setting the result to zero, yields the optimal grating vector component

$$K_{x_h}(x) = \frac{-1}{(a_2(x) - a_1(x))} \int_{a_1(x)}^{a_2(x)} (\hat{K}_{x_d}(x, a) - \hat{K}_{x_i}(x, a)) \, da. \tag{10}$$

Since the second derivative of e^2 is greater than zero, the optimal grating vector yields minimum e^2. Now, the corresponding optimal grating function can be found by using equation (3), as

$$\psi_h(x) = \frac{2\pi}{\lambda} \int K_{x_h}(x) \, dx. \tag{11}$$

For an on-axis holographic element, having circular symmetry, it is possible to approximate the two-dimensional grating function, by one-dimensional on-axis design

$$\psi_h(x, y) = \psi_h(r) = \frac{2\pi}{\lambda} \int K_{r_h}(r) \, dr \tag{12}$$

where $r = \sqrt{x^2 + y^2}$. For an off-axis HOE, where the off-axis angle, θ_r, is relatively low, it is possible to obtain an approximate solution by simply adding a linear term to the on-axis design, to get

$$\psi_h(x, y) = (\psi_h(r))_{\text{on-axis}} + \frac{2\pi}{\lambda} \alpha_r x \tag{13}$$

where $\alpha_r = \sin\theta_r$. Finally it is possible to obtain better approximations for general two-dimensional grating functions, but at the price of added complexity [6].

3. Optimal holographic focusing element

The operation of an on-axis focusing element is described with the aid of the one-dimensional representation in figure 1. Here each input plane wave converges, at the output plane, to a point whose location corresponds to the angular direction of the input wave. The holographic focusing element (HFE) has an aperture of 2D and a focal length f, which is the distance from the holographic element to the stop aperture and to the output plane, and it is centred along the optical axis z. It also has an input stop aperture of $2W$.

It is convenient for focusing element design to let the input parameter, a, be the direction cosine of the input plane wave, so

$$a = \alpha = \sin\theta_i. \tag{14}$$

Consequently, the normalised propagation vector of the input rays is

$$\hat{K}_{x_i}(x, a) = \hat{K}_{x_i}(\alpha) = \alpha. \tag{15}$$

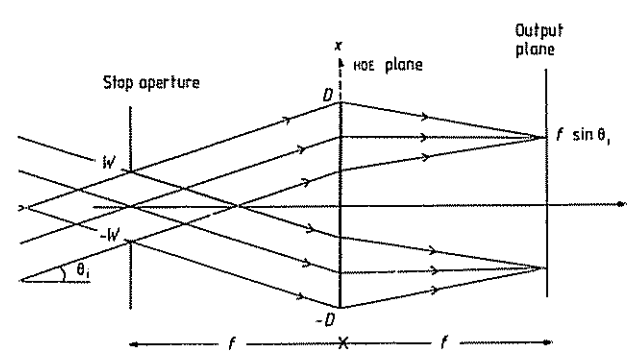

Figure 1. The readout geometry for an on-axis HFE.

Now, an input plane wave, having a direction cosine α, must be transformed into a spherical wave converging to a point αf. Thus, the direction cosines of the desired output rays become

$$\hat{K}_{x_d}(x, a) = \hat{K}_{x_d}(x, \alpha) = \frac{-(x-\alpha f)}{\sqrt{(x-\alpha f)^2 + f^2}}. \quad (16)$$

Substituting $\hat{K}_{x_i}$ from (15) and $\hat{K}_{x_d}$ from (16) into (10), yields

$$K_{x_h}(x) = \frac{-1}{(\alpha_2(x) - \alpha_1(x))} \int_{\alpha_1(x)}^{\alpha_2(x)} \left(\frac{-(x-\alpha f)}{\sqrt{(x-\alpha f)^2 + f^2}} - \alpha \right) d\alpha \quad (17)$$

where $\alpha_1(x)$ and $\alpha_2(x)$ are the lower and upper direction cosines of the input plane waves that intercept the holographic element at a point x.

The solution of (17) provides the final holographic grating vector as

$$K_{x_h}(x) = \frac{\alpha_1(x) + \alpha_2(x)}{2} - \frac{1}{(\alpha_2(x) - \alpha_1(x))} [\sqrt{(x/f - \alpha_2(x))^2 + 1} - \sqrt{(x/f - \alpha_1(x))^2 + 1}]. \quad (18)$$

The lower direction cosine $\alpha_1(x)$ is given by

$$\alpha_1(x) = \frac{x - W}{\sqrt{(x-W)^2 + f^2}} \quad (19a)$$

when

$$\alpha_1(x) > \frac{(-D+W)}{\sqrt{(-D+W)^2 + f^2}} = \alpha_{\min}$$

otherwise

$$\alpha_1(x) = \alpha_{\min}. \quad (19b)$$

The upper direction cosine $\alpha_2(x)$ is given by

$$\alpha_2(x) = \frac{x + W}{\sqrt{(x+W)^2 + f^2}} \quad (20a)$$

when

$$\alpha_2(x) < \frac{(D-W)}{\sqrt{(D-W)^2 + f^2}} = \alpha_{\max}$$

otherwise

$$\alpha_2 = \alpha_{\max}. \quad (20b)$$

For simplicity, it is possible to expand (18) by a Taylor expansion, assuming the paraxial approximation for large f/x. The resulting expansion reveals that the third-order term as well as all even-order terms are zero. This yields a simplified holographic grating vector as

$$(K_{x_h}(x))_{\text{simplified}} = \frac{x}{f} + O((x/f)^5). \quad (21)$$

The dominant first-order term leads to a quadratic focusing element. Finally, using (12) and (13), we find that the grating function for an off-axis focusing element is

$$\psi_h(x, y) = \frac{2\pi}{\lambda} \left(\frac{x^2 + y^2}{2f} + \alpha_r x \right). \quad (22)$$

The readout geometry for such an off-axis element is shown in figure 2, where all the parameters in the figure have been described earlier.

To evaluate the performance of the quadratic off-axis focusing element, given in equation (22), we performed a ray tracing analysis [7], using equations (4)–(6); the parameters of the element were chosen as $f = 100$ mm, $W = 5$ mm, $D = 15$ mm, and $\theta_r = 20°$. The results of the analysis, which do not take into account the diffraction from the aperture, are given as spot diagrams in figure 3(*a*) for nine discrete input angles $(\theta_{x_i}, \theta_{y_i})$. For comparison we also performed a ray-tracing analysis on a conventional holographic spherical element having the same parameters, for which

$$(\psi_h(x, y))_{\text{sph}} = \frac{2\pi}{\lambda} (\sqrt{x^2 + y^2 + f^2} + \alpha_r x). \quad (23)$$

The spot diagrams for the spherical element are given in figure 3(*b*). As shown, except for the central point, where the recording and readout geometries are identical for the spherical element, the results for the quadratic element are uniformly superior. Relatively small spot diagrams are obtained in the quadratic element, even at the extreme angles. We also calculated the amount of distortion by subtracting the actual (average) location of each spot from the desired location; the desired focusing location of the input plane wave at θ_{x_i} is $(\alpha - \alpha_r)f$. Figure 4 shows the distortion as a function of the input angle, θ_{x_i}, for the one-dimensional calculation. As shown, the distortions for the quadratic element are significantly smaller than those for the spherical element.

Using third-order aberrations analysis, we found that for the spherical element of equation (23), the spherical aberrations are zero but the other aberrations, such as coma, astigmatism and distortions, increase rapidly as the input angles increase [6]. For the quadratic element of (22), on the other hand, the spherical aberrations are somewhat larger, but all the other aberrations have been significantly decreased. The sum total of the aberrations for the quadratic design is evidently much better than for the spherical design. The diameter of the spot for a low off-axis angle quadratic element, which is determined by the dominant spherical aberration, is

$$D_{ab} \simeq W^3/f^2. \quad (24)$$

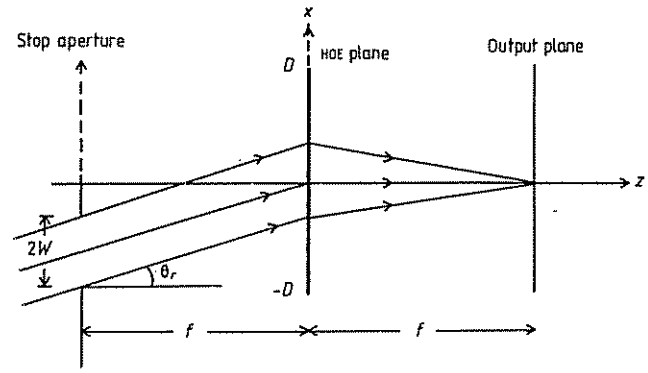

Figure 2. The readout geometry for an off-axis HFE.

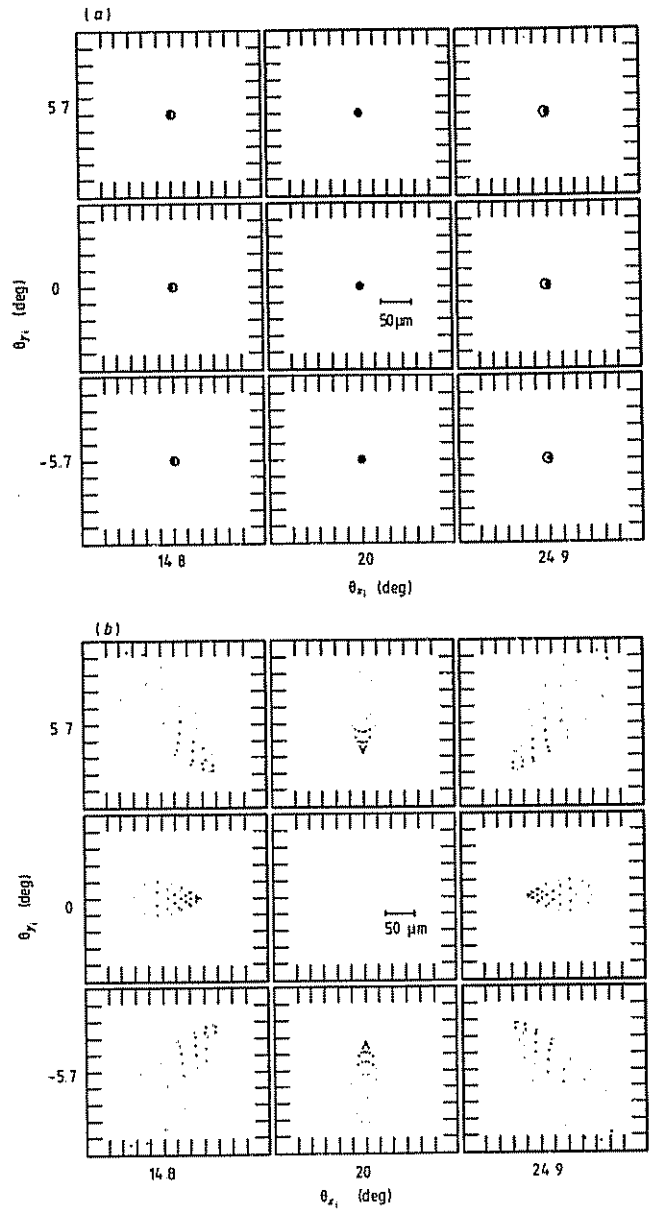

Figure 3. Spot diagrams for the off-axis HFE. (*a*) Quadratic grating function; (*b*) spherical grating function.

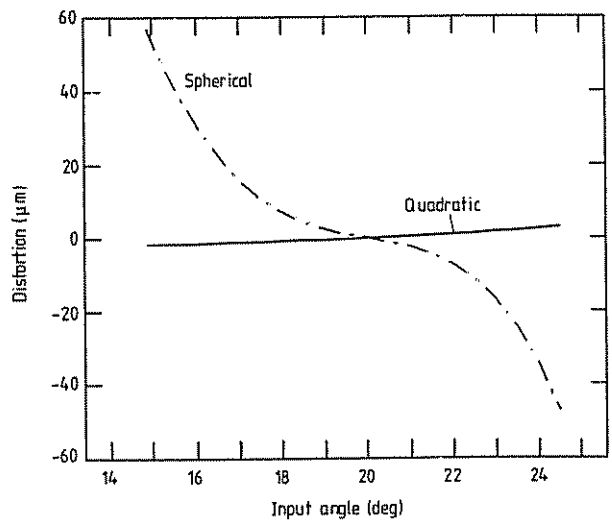

Figure 4. The distortion as a function of input angle, θ_{xi}, for the quadratic and spherical grating functions.

For nearly diffraction-limited performance, we must ensure that D_{ab} is less than the diffraction limited spot size of $2.44\lambda f/2W$. Consequently, the diffraction-limited performance criterion can be given by

$$1.22\lambda f^3/W^4 > 1. \tag{25}$$

Thus, in our specific example of $\lambda = 10.6$ μm and $f =$ 100 mm, the input aperture ($2W$) should be limited to about 20 mm.

4. Realising the focusing element

In order to obtain the holographic focusing element, we used the grating function of equation (22) to first plot a Lee-type [8] binary CGH having the same parameters as those described in the preceding section. The amplitude transmittance of the CGH is given by

$$t_a = U_s[\cos(\psi_h(x, y))]. \tag{26}$$

The term U_s is a unit step function defined by

$$U_s(\xi) = \begin{cases} 1 & \xi \geqslant 0 \\ 0 & \xi < 0. \end{cases} \tag{27}$$

The binary CGH was plotted with a laser scanner (Scitex Raystar, Response 300)† directly onto photographic emulsion; the resolution capabilities are about 10 μm. The binary CGH plot was then demagnified optically (four times) and recorded as a chrome master mask. The information from the mask was transferred by contact printing and suitable exposure onto a glass substrate coated with aluminum and a thin layer of photoresist. After developing the photoresist, the aluminum was etched and the remaining photoresist was removed. Finally, in order to obtain a highly reflective final element the etched aluminum layer was coated with a gold layer. Figure 5 shows an electron microscope picture of a typical etched section of the modulated surface that was obtained. In the scalar approximation [9], the reflectance $H(x, y)$ of the HOE can

† Scitex Corporation, Herzlia B 46103, Israel.

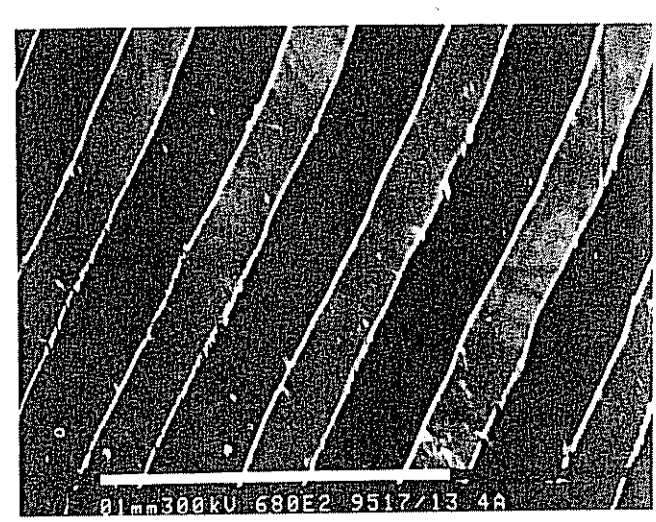

Figure 5. Typical etched section of a modulated surface of the HFE. The white line extends over 100 μm.

be described as

$$H(x, y) \simeq \exp\left[\mathrm{i}\left(\frac{4\pi d}{\lambda} t_a(x, y)\right)\right] \qquad (28)$$

where t_a is given by (26) and d is the depth of the surface modulation. By setting $d \simeq \lambda/4$, it is possible to obtain the maximum efficiency for the relevant first diffracted order (proportional to $\exp(\mathrm{i}\psi_h(x, y))$) from the element [9].

The focusing element was tested with a CO_2 laser at a wavelength of 10.6 μm. The focused spot sizes were measured for various input plane waves by using the scanning knife-edge method [10]. Two stepper motors were used; one for moving the knife-edge and the other for changing the distance, d_{out}, from the holographic element to the measurement plane. Figure 6 shows a representative result for the relative power as a function of the displacement of the knife edge for an input plane wave at $\theta_{x_i} = 24.9°$, $\theta_{y_i} = 0°$. Initially, the knife edge does not block any of the focusing light so the total power is high. As it scans across the focused spot, it blocks more of the light. The spot size was found by first differentiating the curve of figure 6 and then calculating the standard deviation, σ, of the resulting distribution. In our calculations the spot sizes were taken as 4σ. The measurements were performed for the entire range of input angles, $14.8° < \theta_{x_i} < 24.9°$, $-5.7° < \theta_{y_i} < 5.7°$, and we found that the spot sizes were uniformly equal to the diffraction limit, $D_{DL} = 2.44\lambda f/2W \simeq 260$ μm ($f = 100$ mm, $W = 5$ mm).

In the realisation procedure, there are several factors that can deteriorate the optical performance of the holographic element; the quantisation of the grating function by the laser scanner, the aberrations of the optical demagnification system, and the photolithographic process. Note that for the focusing element described above, the thinnest line of the grating function, contains only four demagnified pixels of the laser scanner. Nevertheless, these factors did not significantly degrade the performance of our element, as we realised diffraction-limited performance for the entire range of input angles.

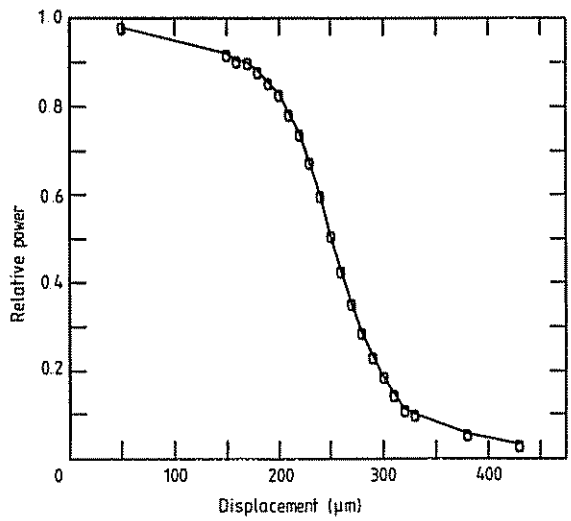

Figure 6. Relative light power as a function of the displacement of the knife edge at the focusing plane for one input plane wave at $\theta_{x_i} = 24.9°$, $\theta_{y_i} = 0°$.

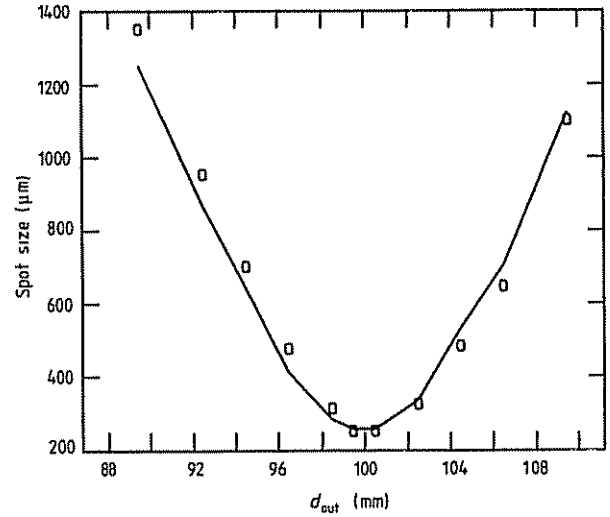

Figure 7. The spot size as a function of the distance, d_{out}, between the hologram and the measurement plane ($\theta_{x_i} = 20°$, $\theta_{y_i} = 0°$). The experimental data is given by the rectangles and the full curve represents the calculated results.

Figure 7 shows the spot size as a function of the distance d_{out} between the hologram and the measurement plane for one input plane wave at $\theta_{x_i} = 20°$, $\theta_{y_i} = 0°$; the experimental data is given by the rectangles. Also shown (the full curve) are the calculated spot sizes determined by the convolution between the geometric aberrations and the diffraction from the input aperture [11]; the geometric aberrations were found by ray-tracing analysis and approximated as Gaussian distributions. As evident, the calculated and experimental results are in good agreement.

5. Concluding remarks

In this paper, we have shown that it is possible to design and realise holographic focusing elements for far-IR having diffraction-limited performance and small distortion over a broad range of incidence angles. For a limited range of incidence angles and for a relatively low off-axis angle, it is sufficient to use the approximate quadratic solution for the focusing element. However, for a larger range of incidence angles, smaller f numbers, and greater off-axis angles, it is necessary to resort to the more complete solution in order to achieve optimum performance.

References

[1] Gallagher N C and Sweeney D W 1979 Infrared holographic optical elements with applications to laser material processing *J. Quantum Electron.* **15** 1369
[2] Lee W H 1980 Techniques for recording holographic lenses for infrared wavelengths *Opt. Commun.* **34** 29
[3] Sweeney, D W, Stevenson W H and Gallagher N C 1980 Holography at 10.6 μm *SPIE* **215** 183

[4] Swanson G J and Veldkamp W B 1985 Binary lenses for use at 10.6 micrometers *Opt. Eng.* **24** 791
[5] Hasman E, Davidson N and Friesem A A 1988 Optimal design for holographic focussing elements *Rev. Roum. Physique* **33** 663
[6] Hasman E and Friesem A A 1989 Analytic optimization for holographic optical elements *J. Opt. Soc. Am.* A **6** 62
[7] Latta J N 1971 Computer-based analysis of holography using ray-tracing *Appl. Opt.* **10** 2698
[8] Lee W H 1974 Binary synthetic holograms *Appl. Opt.* **13** 1677
[9] Campbell D K and Sweeney D W 1978 Materials processing with CO_2 laser holographic scanner systems *Appl. Opt.* **17** 3727
[10] Arnaud J A, Hubbard W M, Mandeville G D, de la Glaviére B, Franke E A and Franke J M 1977 Technique for fast measurement of gaussian laser beam parameters *Appl. Opt.* **10** 2775
[11] Goodman J W 1968 *Introduction to Fourier Optics* (New York: McGraw-Hill)